



# Preparation of Pd-Fe/graphene catalysts by photocatalytic reduction with enhanced electrochemical oxidation-reduction properties for chlorophenols



Xiaozhe Song<sup>a</sup>, Qin Shi<sup>a</sup>, Hui Wang<sup>a,\*</sup>, Shaolei Liu<sup>a</sup>, Chang Tai<sup>a</sup>, Zhaoyong Bian<sup>b, \*\*</sup>

<sup>a</sup> College of Environmental Science and Engineering, Beijing Forestry University, Beijing 100083, PR China

<sup>b</sup> College of Water Sciences, Beijing Normal University, Beijing 100875, PR China

## ARTICLE INFO

### Article history:

Received 25 July 2016

Received in revised form 2 October 2016

Accepted 12 October 2016

Available online 14 October 2016

### Keywords:

Photocatalytic synthesis

Pd-Fe/graphene catalyst

Chlorophenols

Oxygen reduction reaction

Electrochemical reduction-oxidation

## ABSTRACT

A convenient method based on photocatalytic reduction was used to prepare graphene-supported Pd, Fe, and bimetallic Pd-Fe nanoparticle (NP) catalysts under mild conditions. The obtained catalysts were characterized by X-ray diffraction (XRD), scanning electron microscopy (SEM), transmission electron microscopy (TEM), atomic force microscopy (AFM), and X-ray photoelectron spectroscopy (XPS). Their potential application to the electrocatalytic degradation of chlorinated phenols (CPs) was investigated by cyclic voltammetry (CV) and chronoamperometry. The graphene-supported bimetallic Pd-Fe NP catalyst ( $Pd_{0.5}Fe_{0.5}/graphene$ ) exhibited the optimal surface performance and contained highly abundant and widespread Pd-Fe NPs of approximately  $6.75 \pm 0.05$  nm in size. It exhibited higher electrocatalytic activity for dechlorination of CPs attributed to its higher hydrogen adsorption peak current of  $0.117$  mA than that of the Pd/graphene catalyst, with a 1% weight ratio of Pd ( $Pd_{1.0}/graphene$  catalyst), and the Fe/graphene catalyst, with a 1% weight ratio of Fe ( $Fe_{1.0}/graphene$  catalyst). The highest reductive peak current ( $0.038$  mA) was obtained at  $-0.347$  V when using the  $Pd_{0.5}Fe_{0.5}/graphene$  catalyst, indicating that the  $Pd_{0.5}Fe_{0.5}/graphene$  catalyst has the highest electrocatalytic activity for accelerating the two-electron reduction of  $O_2$  to  $H_2O_2$ . In addition, the electrocatalytic activity was enhanced when feeding with  $O_2$  and at pH 12.8. The electrochemical reductive reaction of  $O_2$  is typically a diffusion-controlled electrochemical process. The calculated values of  $k$  representing the mass transfer rate were in the order  $Pd_{0.5}Fe_{0.5}/graphene$  ( $0.379$ )  $> Pd_{1.0}/graphene$  ( $0.178$ )  $> Fe_{1.0}/graphene$  ( $0.175$ ). The reduction peak currents for four CPs decreased in the order 3-chlorophenol ( $0.0214$  mA)  $> 2,4,5$ -trichlorophenol ( $0.0190$  mA)  $> 2,4$ -dichlorophenol ( $0.0188$  mA)  $> 4$ -chlorophenol ( $0.0178$  mA), indicating that the  $Pd_{0.5}Fe_{0.5}/graphene$  electrode would show the most powerful indirect electro-oxidation for 3-CP degradation in comparison with the other CPs. Therefore, the  $Pd_{0.5}Fe_{0.5}/graphene$  catalyst exhibits a higher electrocatalytic activity than the  $Pd_{1.0}/graphene$  catalyst and  $Fe_{1.0}/graphene$  catalyst for the reductive dechlorination and indirect electrochemical oxidation of CPs.

© 2016 Elsevier B.V. All rights reserved.

## 1. Introduction

Chlorophenols (CPs), generally used in the production of raw materials and pesticides, have been identified as priority pollutants by the US Environmental Protection Agency owing to their high toxicity to organisms including human beings [1,2]. Conventional pollutant control technologies, such as physical, chemical, and bio-

logical treatments, are insufficient to completely dechlorinate CPs [3]. Therefore, development of efficient and economical dechlorination methods is particularly important for CPs treatment.

The advanced electrocatalytic oxidation process has been widely used to treat CPs because of its easy operation, low cost, and high efficiency [4]. The benzene ring is broken during oxidation and generates several possible chlorinated aromatics, which can be more toxic than the initial CPs and are difficult to further degrade [5]. Hence, dechlorination is necessary before the oxidative degradation of organic substances containing chlorine. Alternatively, electrochemical reduction has become an economic pathway for CP treatment with little secondary pollution and excellent dechlorination performance under mild conditions [6]. The mechanism

\* Corresponding author at: PO Box 60, No. 35 Qinghua East Road, Haidian District, Beijing 100083 PR China.

\*\* Corresponding author at: No. 19 XinJieKouWai Street, Haidian District, Beijing 100875 PR China.

E-mail addresses: [wanghui@bjfu.edu.cn](mailto:wanghui@bjfu.edu.cn) (H. Wang), [bian@bnu.edu.cn](mailto:bian@bnu.edu.cn) (Z. Bian).

of electrochemical dechlorination is usually construed as electrochemical hydrogenolysis (ECH), in which activated hydrogen ( $H^*$ ) generated from electro-reduction on the cathode attacks the C–Cl bonds [7]. However, ECH of CPs can produce numerous non-biodegradable organics such as phenol. After dechlorination, the CPs is transformed to intermediate products with phenol structures that require further degradation; however, the further removal of intermediate products may be easily ignored at present [8]. Thus, a combined process of electrocatalytic reduction and oxidation of CPs has become an efficient route to achieve complete dechlorination and mineralization of CPs [9,10].

Carbon materials are often employed as support materials for degradation of CPs owing to their large surface area, high porosity, and comparatively good electrical conductivity. Graphene has proved to be an excellent material for reinforcing nanocomposites compared to graphene [11]. Furthermore, graphene has attracted considerable attention as an alternative to other carbon materials because of its remarkable supporting matrix and excellent electronic conductivity [12,13]. Currently, the combination of metal nanoparticles (NPs) and graphene sheets as cathode materials is an attractive strategy for chlorinated organic compound treatment, since the introduction of metal NPs into graphene sheets can effectively mitigate the aggregation of metal NPs and improve their electrocatalytic properties [13–15].

Pd NPs are the preferred material for ECH because of their superior ability to adsorb hydrogen and excellent electrical conductivity [12,16]. However, Pd metal is expensive and unstable, and bimetallic systems possess superior electrocatalytic abilities to monometallic systems [17]. Bimetallic Pd/Fe nanocomposites, compared with other bimetallic systems formed with Pd, such as Pd/Sn, Pd/Au, and Pd/Ni, have been reported to have excellent dechlorination activities for CPs [18–22]. The addition of Fe NPs to Pd for the dechlorination process has been confirmed to promote the stability of Pd, which provides a larger area electrochemical surface for the active Pd [10]. Furthermore, a Pd-Fe bimetallic catalyst has been reported to exhibit remarkable catalytic properties and a high dechlorination efficiency [16].

Graphene modified by metal NPs can be produced by various methods, such as chemical reduction processes, hydrothermal techniques, electrodeposition, and traditional incipient wetness impregnation [23–27]. However, most of these methods suffer from complex experimental procedures, high temperatures in hydrothermal synthesis, and the various highly toxic reducing agents required. These problems can also cause the electron transfer capacity and catalytic activity of the materials to decrease [13,28]. Therefore, development of a facile and green route to prepare these catalysts is highly desirable. Photocatalytic reduction, deemed to be a milder and greener method than conventional reduction processes, can not only form graphene sheets rapidly but also activate the electronic contact between the graphene sheets and metal NPs [29–34]. Photocatalytic reduction is commonly accomplished with photocatalysts such as titanium oxide ( $TiO_2$ ), zinc oxide ( $ZnO$ ), and phosphotungstic acid ( $H_3PW_{12}O_{40}$ , HPW), which can be easily activated by UV irradiation. Continuous light sensitization can promote the generation of excited states in the photocatalysts through electron transfer, and then these excited states participate in the reduction of graphene oxide (GO) or metal ions and convert them back into their original states [29,30].  $TiO_2$  and  $ZnO$  NPs as UV-absorptive photocatalysts have been used to prepare graphene loaded with metal particles, but may cause the formation of the impure oxide. Compared with  $ZnO$  and  $TiO_2$ , HPW has lower reduction power but the same reduction effects under UV irradiation, and thus is usually used as a selective photocatalytic reductant [31–33]. Moom et al. [33] demonstrated synthesis of graphene as a suspension with HPW and UV-irradiation firstly, and then the metal precursors reacted with graphene to form hybrids

of Ag, Au, and Pd/graphene in dimethyl formamide (DMF) solution. To obtain higher load rate and brief procedure, Pasricha et al. [34] pointed out the synchronous reduction of GO and metal precursors with HPW under the UV-light irradiation. However, the preparation process of bimetallic NPs supported on graphene sheets with light-irradiation and their electrocatalytic properties has been rarely reported. Hence, we synthesized bimetallic NPs/graphene under light-irradiation. This method is easier and efficient compared with the traditional ones. The prepared bimetallic NPs/graphene showed competitive properties. The most distinct features in this study could be concluding two points: (1) unique method to support bimetallic NPs, which completely synchronized with GO reduction to graphene. (2) not only characterization analysis, subsequent electrocatalytic activities for CPs degradation were also studied.

In this study, Pd/graphene, Fe/graphene, and Pd-Fe/graphene catalysts were synthesized and then investigated for their electrochemical activities in the degradation of CPs. Firstly, catalysts with different loadings of metal particles were prepared through UV-irradiation reduction of GO and metal precursors with HPW as the reducing agent. The morphology and composition changes of the catalysts were investigated by X-ray diffraction (XRD), transmission electron microscopy (TEM), atomic force microscopy (AFM), and X-ray photoelectron spectroscopy (XPS). Electrochemical measurements, including cyclic voltammetry (CV) and chronoamperometry, were performed to assess electrocatalytic activities of the catalysts in the degradation of CPs, and their potential operating conditions.

## 2. Experimental

### 2.1. UV-irradiation synthesis of catalysts

GO was obtained from powdered graphite according to a modified Hummers' method [35,36]. Graphene sheets decorated with different loadings of Pd, Fe, and Pd-Fe NPs were prepared by improved photocatalytic reduction with HPW [33,34]. GO (100 mg) was added to 200 mL ultrapure water (resistivity  $>18.2\text{ M}\Omega$ ) and placed in a bath sonicator for 30 min. Then,  $0.1\text{ mol L}^{-1}$  NaOH solution was added dropwise to adjust the pH to  $\sim 7$ . The stable dispersion was equally split into eight portions and placed in quartz tubes. HPW (3 mL,  $10\text{ mg mL}^{-1}$ ) solution was first added dropwise to each quartz tube and then 10 mL isopropyl alcohol ( $Me_2CHOH$ ) was added. After stirring for 30 min with a magnetic stirrer, the appropriate volumes of  $0.2\text{ mg mL}^{-1}$   $PdCl_2 \cdot 6H_2O$  and  $0.2\text{ mg mL}^{-1}$   $FeCl_3 \cdot 6H_2O$  aqueous solutions were dropped into the mixture and continually stirred for 1.5 h. The mixed solution was irradiated with a high-pressure mercury lamp (365 nm) for 3 h with constant stirring. The precipitation obtained was washed with isopropyl alcohol and deionized water thoroughly until the pH of the solution reached 7. Then, the as-obtained samples were dried under vacuum for 2 h and stored after grinding. The synthesis of graphene-supported Pd NP catalysts ( $Pd_x/\text{graphene}$ ) and graphene-supported Fe NP catalysts ( $Fe_x/\text{graphene}$ ) were conducted by the same procedure, where X indicates the weight ratio of metal to graphene sheets.

### 2.2. Characterization methods

XRD was carried out to analyze the crystal structures using an X'Pert PRO MPD X-ray powder diffractometer (PANalytical B.V., Holland) with Cu radiation between  $5^\circ$  and  $80^\circ$  at a scan rate of  $4^\circ/\text{min}$  and an incident wavelength of  $0.15406\text{ nm}$  ( $Cu K\alpha$ ). The surface morphology of the catalysts with different metal weight ratios were examined using an S-4800 SEM (Hitachi Co., Japan). Images of the catalysts were recorded at different magnifications at operating voltages of 5 kV or 10 kV. TEM images, energy-dispersive

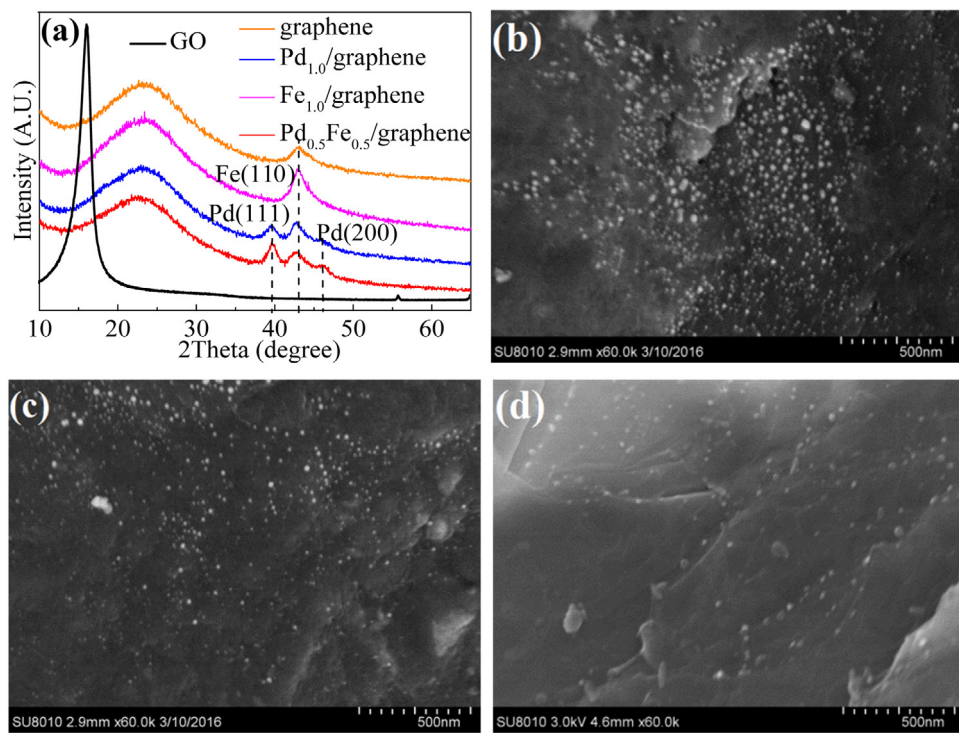


**Fig. 1.** XRD patterns (a) of GO, graphene,  $\text{Pd}_{1.0}/\text{graphene}$ ,  $\text{Fe}_{1.0}/\text{graphene}$  and  $\text{Pd}_{0.5}\text{Fe}_{0.5}/\text{graphene}$  catalysts, SEM images of  $\text{Pd}_{1.0}/\text{graphene}$  (b),  $\text{Fe}_{1.0}/\text{graphene}$  (c) and  $\text{Pd}_{0.5}\text{Fe}_{0.5}/\text{graphene}$  (d) catalysts.

**Table 1**

Loading data of catalysts with different weight ratios measured by XRD and TEM.

| Catalyst (samples)                               | Theoretical loading (wt.%) | Practical loading (wt.%) |      | Particle size (nm) |                 |
|--|----------------------------|--------------------------|------|--------------------|-----------------|
|  |                            | Pd                       | Fe   | XRD                | TEM             |
| $\text{Pd}_{0.5}/\text{graphene}$                | 0.5                        | 0.46                     | /    | 5.42               | /               |
| $\text{Pd}_{1.0}/\text{graphene}$                | 1.0                        | 1.17                     | /    | 6.55               | $6.5 \pm 0.05$  |
| $\text{Pd}_{2.0}/\text{graphene}$                | 2.0                        | 1.93                     | /    | 6.87               | /               |
| $\text{Fe}_{0.5}/\text{graphene}$                | 0.5                        | /                        | 0.51 | 4.86               | /               |
| $\text{Fe}_{1.0}/\text{graphene}$                | 1.0                        | /                        | 1.03 | 6.21               | $6.0 \pm 0.05$  |
| $\text{Fe}_{2.0}/\text{graphene}$                | 2.0                        | /                        | 1.87 | 6.59               | /               |
| $\text{Pd}_{0.5}\text{Fe}_{0.5}/\text{graphene}$ | 0.5–0.5                    | 0.62                     | 0.59 | 6.64               | $6.75 \pm 0.05$ |
| $\text{Pd}_{1.0}\text{Fe}_{1.0}/\text{graphene}$ | 1.0–1.0                    | 0.93                     | 0.89 | 6.87               | /               |
| $\text{Pd}_{2.0}\text{Fe}_{1.0}/\text{graphene}$ | 2.0–1.0                    | 1.84                     | 0.93 | 6.92               | /               |

spectrometry (EDS), and elemental mapping images were taken on a JEM-2010F TEM microscope (Hitachi Co., Japan) at a voltage of 160 kV. EDS was performed at a resolution of 138 eV and the analyzable element range was B5-U92. The surface structures of the catalysts were measured on a SPM-9600 AFM apparatus (Shimazu, Japan) over an area of  $2.5 \times 2.5 \mu\text{m}$ . XPS was performed to ascertain the surface compositions and concentrations of the metal NPs by Model PHI5300 ESCA apparatus (PE-PHI, USA) with Mg K $\alpha$  radiation. The pass energy was 2 min, the operand power was 250 W, and the scan step-size was 5 eV/step.

### 2.3. Electrochemical measurements

All electrochemical measurements (CV and chronoamperometry) were conducted on a CHI 660D electrochemical workstation (Shanghai CH Instrument Company, China) with a three-electrode cell system at room temperature. A platinum rod and a saturated calomel electrode (SCE) were used as counter electrode (3 mm) and reference electrode, respectively. The working electrode was a glassy carbon disk electrode modified with the catalyst (3 mm). The glassy carbon disk electrode was smoothed flat by a sequence

of  $1.0 \mu\text{m}$ ,  $0.3 \mu\text{m}$ , and  $0.05 \mu\text{m}$  alumina on a Master-Tex polishing pad, followed by rinsing thoroughly with ultrapure water. Samples (2.0 mg) were dissolved in 1.0 mL anhydrous ethanol and 50  $\mu\text{L}$  Nafion solution (5%) was added and uniformly mixed. Aliquots (5  $\mu\text{L}$ ) of the solution were removed and dropped onto the glass carbon disk under continuous drying by infrared light. Electrolytes were de-oxygenated with bubbling  $\text{N}_2$  for 30 min prior to each scan. The electrolyte was  $0.5 \text{ mol L}^{-1}$   $\text{Na}_2\text{SO}_4$  solution (pH 7.0, 12.8) in the absence and presence of the CPs, i.e., 4-chlorophenol (4-CP), 3-chlorophenol (3-CP), 2,4-dichlorophenol (2,4-DCP), and 2,4,5-trichlorophenol (2,4,5-TCP), respectively. The original concentration of all CPs was  $100 \text{ mg L}^{-1}$ .

## 3. Results and discussion

### 3.1. Morphological and chemical characterization of metal NPs on graphene sheets

XRD was carried out to identify the components present in the electro-catalysts prepared by UV-assisted photocatalytic reduction. Fig. 1a shows the XRD patterns of  $\text{Pd}_{1.0}/\text{graphene}$ ,

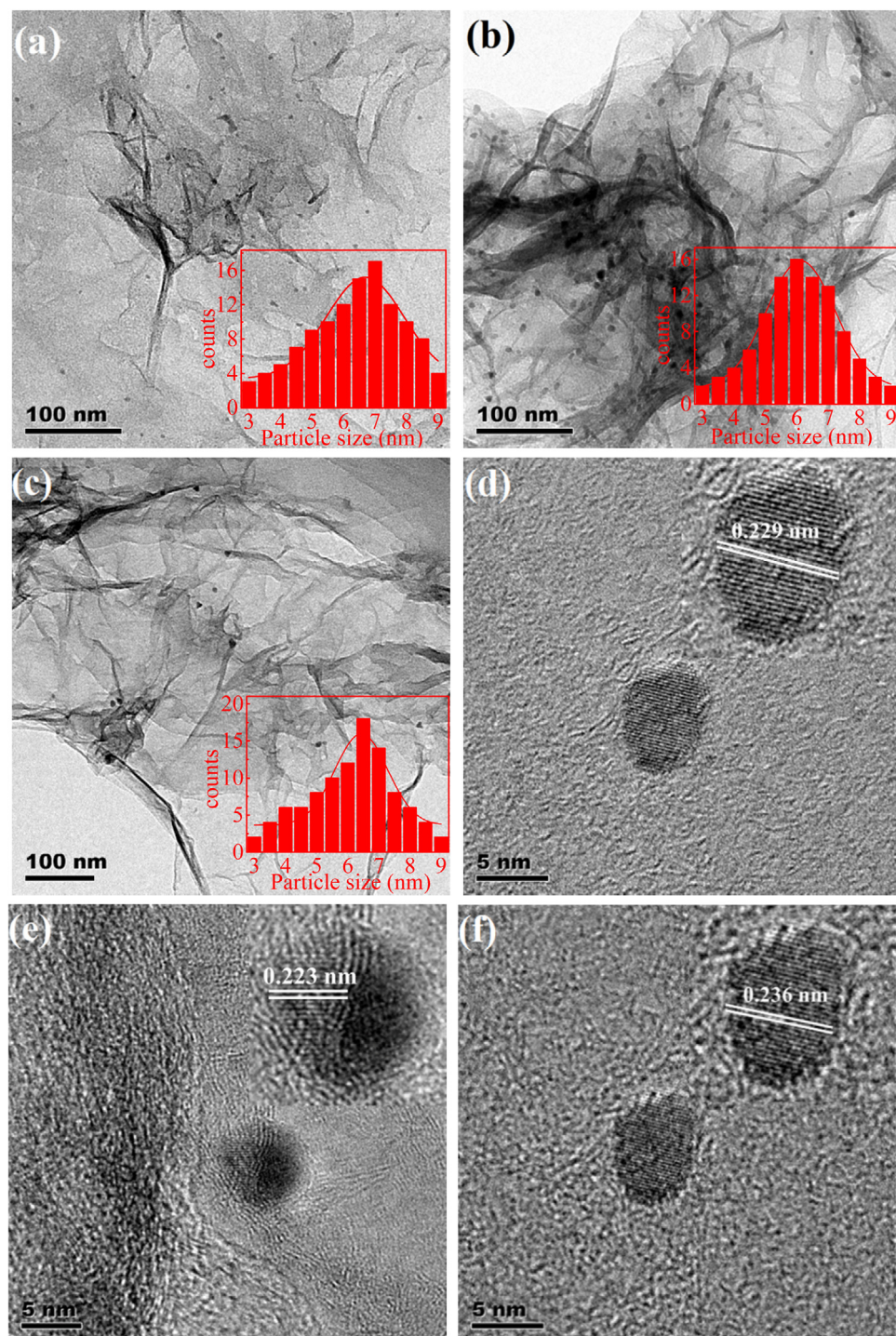


**Fig. 2.** TEM images and particle size distribution analysis (insert) of Pd<sub>1.0</sub>/graphene (a), Fe<sub>1.0</sub>/graphene (b) and Pd<sub>0.5</sub>Fe<sub>0.5</sub>/graphene (c) catalysts, the HR-TEM images of Pd<sub>1.0</sub>/graphene (d), Fe<sub>1.0</sub>/graphene (e) and Pd<sub>0.5</sub>Fe<sub>0.5</sub>/graphene (f) catalysts.

Fe<sub>1.0</sub>/graphene, Pd<sub>0.5</sub>Fe<sub>0.5</sub>/graphene, graphene, and GO. The GO sample exhibits a sharp diffraction peak at 16.3°, corresponding to the (001) reflection of a 0.54 nm interlayer spacing [36]. After reduction with HPW, this sharp peak for GO completely disappears, and the obtained samples all show a broad characteristic peak at about 26.3°, which corresponds to graphene [23]. This indicates that GO is reduced to graphene upon treatment with UV irradiation in the presence of HPW. Two typical diffraction peaks at 42.4° and 49.3° correspond to the (111) and (200) crystal planes of the Pd sample in the Pd<sub>1.0</sub>/graphene catalyst sample according to JCPDS

No. 87-0639. XRD patterns of the Fe<sub>1.0</sub>/graphene catalyst featured a diffraction peak at 46.2°, which attributed to the (110) crystal planes of Fe according to JCPDS No. 87-0721, and overlap with the characteristic peak of the graphene catalyst. However, the presence of Fe could be also confirmed by EDS and XPS data (see below). The peaks at 45.7°, 42.8° and 49.8° for Pd<sub>0.5</sub>Fe<sub>0.5</sub>/graphene catalyst can be assigned to Fe (110), Pd (111) and Pd (200) of Pd-Fe NPs. Compared the patterns of Pd<sub>0.5</sub>Fe<sub>0.5</sub>/graphene catalyst with Pd<sub>1.0</sub>/graphene and Fe<sub>1.0</sub>/graphene catalyst, Fe (110) peak of Pd-Fe NPs shifted to a lower diffraction angle, however, Pd (111)

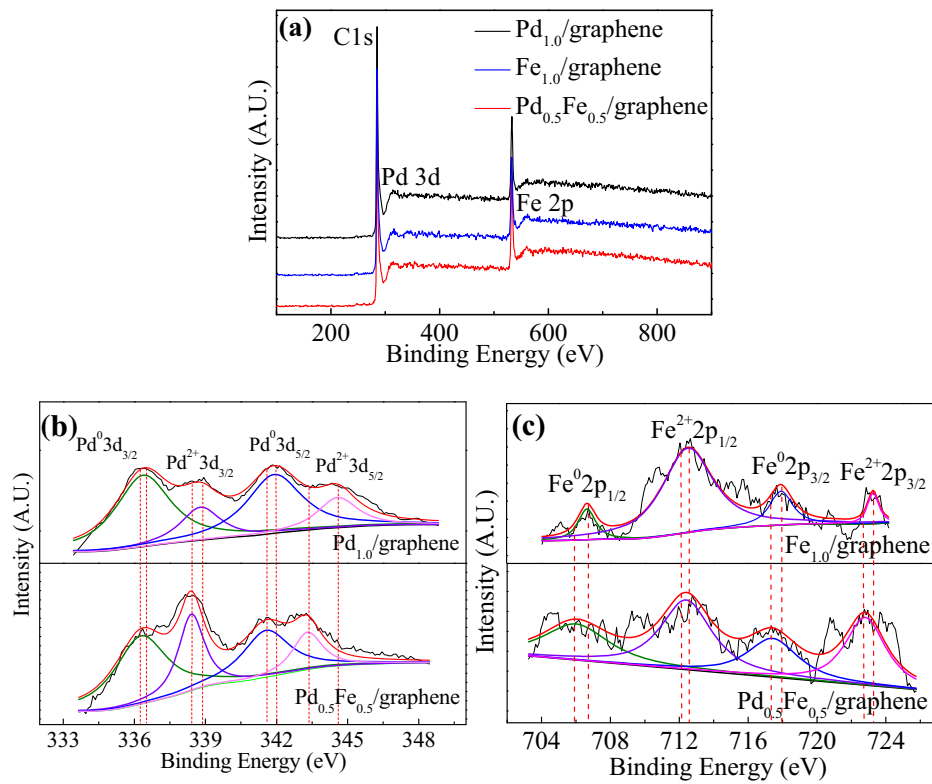


**Fig. 3.** XPS spectra (a) of  $\text{Pd}_{1.0}/\text{graphene}$ ,  $\text{Fe}_{1.0}/\text{graphene}$  and  $\text{Pd}_{0.5}\text{Fe}_{0.5}/\text{graphene}$  catalysts showing the peak for C 1s, Pd 3d and Fe 3p, high-resolution Pd 3d spectra (b) of  $\text{Pd}_{1.0}/\text{graphene}$  and  $\text{Pd}_{0.5}\text{Fe}_{0.5}/\text{graphene}$  catalysts, Fe 3p spectra(c) of  $\text{Fe}_{1.0}/\text{graphene}$  and  $\text{Pd}_{0.5}\text{Fe}_{0.5}/\text{graphene}$  catalysts.

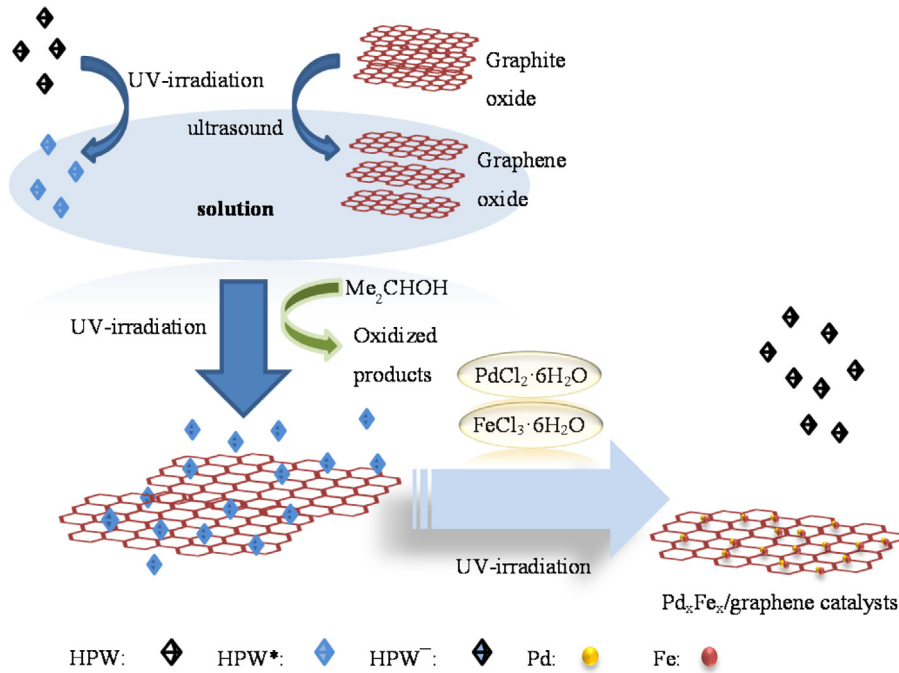


**Fig. 4.** The reaction mechanism for photoreduction synthesis of graphene modified with metal (Pd, Fe, and Pd-Fe) NPs catalysts.

and Pd (200) patterns of Pd-Fe NPs shifted to the higher angle. The peak position offset confirmed the slight change of crystalline interplanar spacing, which attributed to Pd-Fe alloy formation in  $\text{Pd}_{0.5}\text{Fe}_{0.5}/\text{graphene}$  catalyst [14]. These results suggested that metal NPs were successfully deposited on the graphene. The SEM

images of  $\text{Pd}_{1.0}/\text{graphene}$ ,  $\text{Fe}_{1.0}/\text{graphene}$ , and  $\text{Pd}_{0.5}\text{Fe}_{0.5}/\text{graphene}$  show large amounts of the metal NPs appearing as bright white spots distributed on the graphene sheets, as shown in Fig. 1b-d. These catalysts all exhibited a similar distribution of metal NPs. Fig. S1 shows the distribution of metal NPs (Pd, Fe, and bimetallic Pd-Fe)

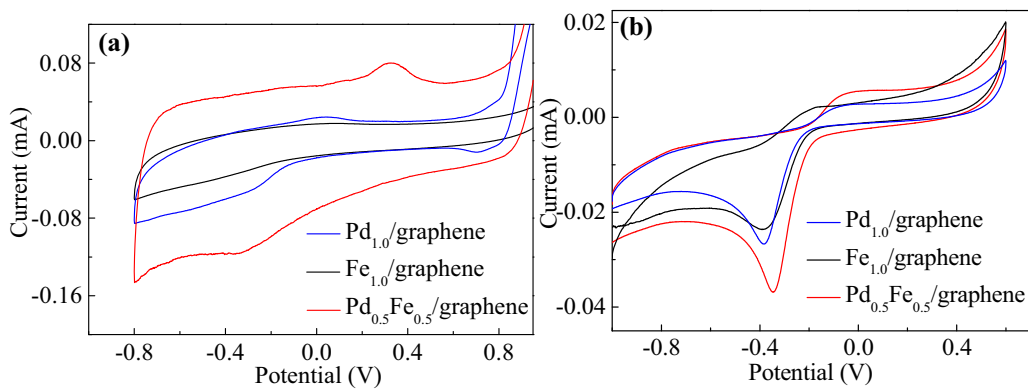


Fig. 5. CV curves of Pd<sub>1.0</sub>/graphene, Fe<sub>1.0</sub>/graphene and Pd<sub>0.5</sub>Fe<sub>0.5</sub>/graphene catalysts in 0.5 mol L<sup>-1</sup> Na<sub>2</sub>SO<sub>4</sub> solution (pH = 12.8) by feeding H<sub>2</sub> (a) and O<sub>2</sub> (b).

in the catalysts with different weight ratios of the dopant metal. It was difficult to detect any metal nanoparticle in the Pd<sub>0.5</sub>/graphene (Fig. S1a) and Fe<sub>0.5</sub>/graphene catalysts (Fig. S1d) owing to their low metal loading. Furthermore, there was significant metal NP aggregation in the Pd<sub>2.0</sub>/graphene (Fig. S1c), Fe<sub>2.0</sub>/graphene (Fig. S1f), Pd<sub>1.0</sub>Fe<sub>1.0</sub>/graphene (Fig. S1h), and Pd<sub>1.0</sub>Fe<sub>2.0</sub>/graphene catalysts (Fig. S1i), owing to their high total metal loading.

More detail can be observed in the TEM images at a scale of 100 nm. As shown in Fig. 2a–c, NPs were clearly observed on the corrugated graphene sheets. Pd-Fe bimetallic NPs assembled on the surface of the graphene nanosheets effectively, and their elementary composition could be confirmed by the corresponding EDS pattern (Fig. S2), which is more intense than that of the monometallic NPs in the Pd<sub>1.0</sub>/graphene and Fe<sub>1.0</sub>/graphene catalysts. It is noteworthy that the NPs were better dispersed after the addition of Fe, which may result from its modification of the Pd NPs [21]. Meanwhile, SEM-EDS mapping of Pd<sub>0.5</sub>Fe<sub>0.5</sub>/graphene catalyst (Fig. S3) was tested to confirm the atom dispersion of NPs. Combined the SEM, TEM images and mapping results, we can draw a conclusion that Pd<sub>0.5</sub>Fe<sub>0.5</sub>/graphene catalyst exhibited a similar distribution of metal NPs than Pd<sub>1.0</sub>/graphene and Fe<sub>1.0</sub>/graphene catalysts. According to the corresponding particle size distribution histogram (Fig. 2d–f), the average size of the Pd-Fe bimetallic NPs in the Pd<sub>0.5</sub>Fe<sub>0.5</sub>/graphene catalyst was 6.75 ± 0.05 nm, similar to that in the Pd<sub>1.0</sub>/graphene catalyst (6.5 ± 0.05 nm), and slightly larger than that in the Fe<sub>1.0</sub>/graphene catalyst (6.0 ± 0.05 nm). And similar Pd-Fe/graphene catalyst (Pd:Fe = 1:1) was synthesized by chemical reduction with size of 5.2 ± 0.3 nm [10]. The average deflection of particle size in two different synthetic methods proved that Pd-Fe NPs synthesized by photo reduction was more homogeneous and uniform than that by the traditional chemical reduction.

Moreover, compared with the electrodeposition method [24,25], traditional incipient wetness impregnation [22], and the chemical reduction method [26,27], the bimetallic Pd-Fe NPs obtained by UV-assisted photocatalytic reduction are superior to the majority of them in the particle size and related properties. It indicated that the Pd<sub>0.5</sub>Fe<sub>0.5</sub>/graphene catalyst prepared by UV-irradiation reduction might provide higher electrocatalysis activities attributed to the small size and uniform of the catalyst nanoparticles and promotion effect by HPW than those prepared by other methods [34]. The lattice spacing in the Pd<sub>0.5</sub>Fe<sub>0.5</sub>/graphene catalyst was 0.229 nm (Fig. 2d), which was larger than the calculated value for the (111) planes of Pd in the Pd<sub>1.0</sub>/graphene catalyst (Fig. 2e) and lower than the (110) planes of Fe in the Fe<sub>1.0</sub>/graphene catalyst (Fig. 2f). It indicated Pd-Fe alloy formation in the Pd<sub>0.5</sub>Fe<sub>0.5</sub>/graphene catalyst sample [14,37]. The typical AFM image of the Pd<sub>0.5</sub>Fe<sub>0.5</sub>/graphene catalyst shown in Fig. S4 revealed that this hybrid is an irregular crystal block with an average thickness of approximately 1.2 nm. The average roughness of the sheets is 0.175 nm. This rough surface is characteristic of the formation of bimetallic Pd-Fe NPs and provides a larger number of active sites.

In order to further understand the modification caused by Fe addition, the sizes of the metal NPs in the corresponding catalysts are shown in Table 1, which were calculated using the Scherrer equation based on the XRD images (Fig. S5). As can be seen in Table 1, the Pd crystallite sizes in the Pd<sub>0.5</sub>/graphene, Pd<sub>1.0</sub>/graphene, and Pd<sub>2.0</sub>/graphene catalysts are about 5.42, 6.55, and 6.87 nm, respectively. The Pd NP crystallite size increased with an increase in loading weight ratio. A similar trend was observed for the Fe/graphene and Pd-Fe/graphene catalysts. It was noted that the sizes of the metal NPs in the Pd-Fe/graphene catalysts are 6.64 nm (Pd<sub>0.5</sub>Fe<sub>0.5</sub>/graphene), 6.87 nm (Pd<sub>1.0</sub>Fe<sub>1.0</sub>/graphene), and 6.92 nm (Pd<sub>2.0</sub>Fe<sub>1.0</sub>/graphene), which is in agreement with the results of

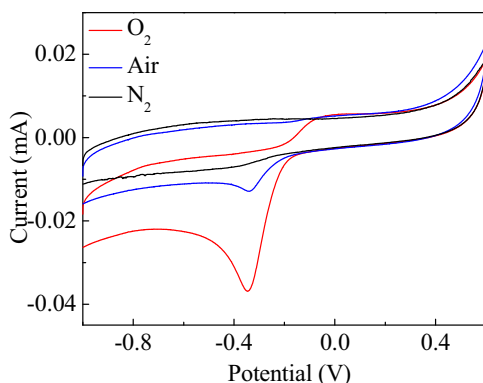


Fig. 6. CV curves of Pd<sub>0.5</sub>Fe<sub>0.5</sub>/graphene catalyst in 0.5 mol L<sup>-1</sup> Na<sub>2</sub>SO<sub>4</sub> solution (pH = 12.8) by feeding N<sub>2</sub>, air and O<sub>2</sub>, repectively.

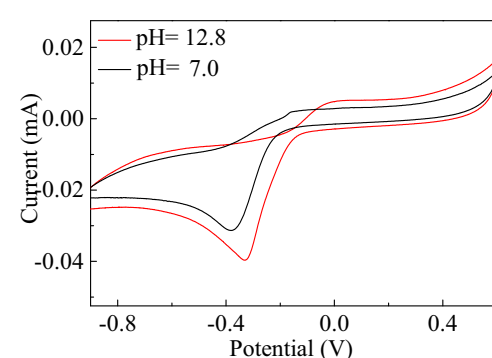
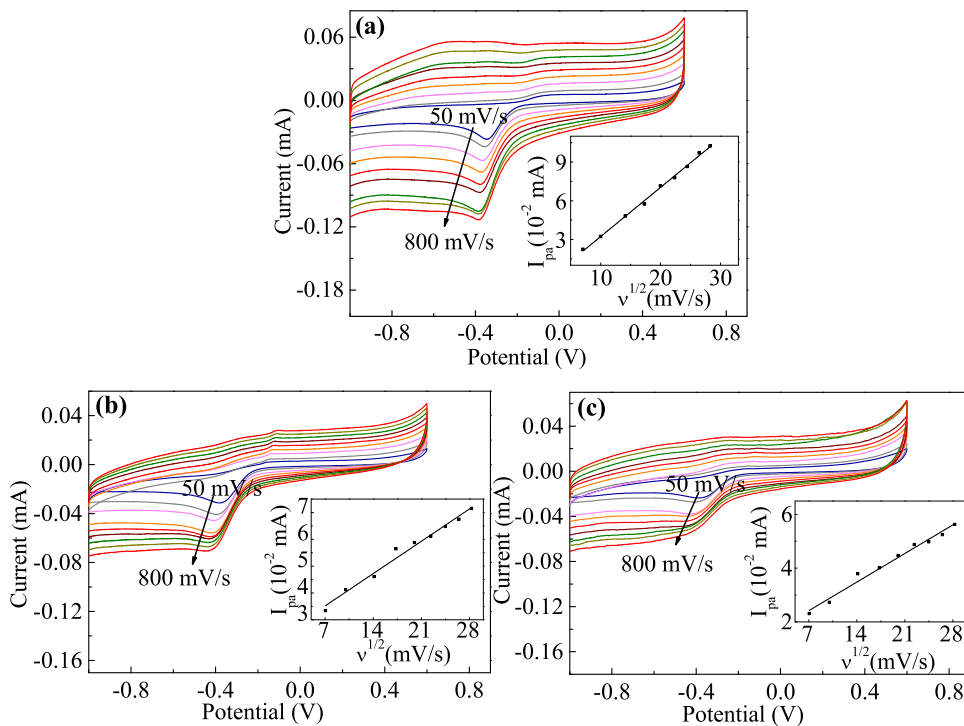


Fig. 7. CV curves of Pd<sub>0.5</sub>Fe<sub>0.5</sub>/graphene catalyst in neutral solution (0.5 mol L<sup>-1</sup> Na<sub>2</sub>SO<sub>4</sub> + pH = 7.0) and alkaline solution (0.5 mol L<sup>-1</sup> Na<sub>2</sub>SO<sub>4</sub> + pH = 12.8).



**Fig. 8.** CV curves and the plot of peak currents vs. the square root of scan rates (insert) of  $\text{Pd}_{1.0}/\text{graphene}$ ,  $\text{Fe}_{1.0}/\text{graphene}$  and  $\text{Pd}_{0.5}\text{Fe}_{0.5}/\text{graphene}$  catalysts in  $0.5 \text{ mol L}^{-1} \text{Na}_2\text{SO}_4$  solution ( $\text{pH} = 12.8$ ) using  $\text{O}_2$  under different scan rates:  $50 \text{ mV s}^{-1}$ ,  $100 \text{ mV s}^{-1}$ ,  $200 \text{ mV s}^{-1}$ ,  $300 \text{ mV s}^{-1}$ ,  $400 \text{ mV s}^{-1}$ ,  $500 \text{ mV s}^{-1}$ ,  $600 \text{ mV s}^{-1}$ ,  $700 \text{ mV s}^{-1}$ ,  $800 \text{ mV s}^{-1}$ .

the TEM analyses. The  $\text{Pd}_{0.5}\text{Fe}_{0.5}/\text{graphene}$  catalyst presented the smallest metal NPs. A slight increase in the NPs size in comparison with the corresponding  $\text{Pd}/\text{graphene}$  catalyst was observed when elemental Fe was added. In conclusion, modification with an appropriate amount of Fe improves the dispersion of the NPs but does not significantly affect their size.

Systematic XPS investigations were conducted to provide further insight into the surface chemistry of the  $\text{Pd}_{1.0}/\text{graphene}$ ,  $\text{Fe}_{1.0}/\text{graphene}$ , and  $\text{Pd}_{0.5}\text{Fe}_{0.5}/\text{graphene}$  catalysts. The results showed significant C signals, Pd 3d signals, and Fe 2p signals in the XPS spectra of the different catalysts (Fig. 3a). The Pd 3d region of the XPS spectra of  $\text{Pd}_{1.0}/\text{graphene}$  and  $\text{Pd}_{0.5}\text{Fe}_{0.5}/\text{graphene}$  are depicted in Fig. 3b.  $\text{Pd}_{1.0}/\text{graphene}$  presents characteristic Pd  $3d_{3/2}$  and Pd  $3d_{5/2}$  peaks with banding energies at 341.90 and 336.37 eV, respectively, which indicate the presence of metallic  $\text{Pd}^0$  loaded onto the graphene. The second pair of Pd signals appearing at 344.58 and 338.78 eV was attributed to Pd atoms with lower charge density ( $\text{Pd}^{2+}$ ). The  $\text{Pd}_{0.5}\text{Fe}_{0.5}/\text{graphene}$  catalyst presents peaks characteristic of Pd  $3d_{3/2}$ ,  $\text{Pd}^0$   $3d_{5/2}$ ,  $\text{Pd}^{2+}$   $3d_{3/2}$ , and  $\text{Pd}^{2+}$   $3d_{5/2}$  at 341.55, 336.28, 343.3, and 338.4 eV, respectively. The binding energies of Pd 3d and Fe 2p in the  $\text{Pd}_{0.5}\text{Fe}_{0.5}/\text{graphene}$  catalyst shifted to lower energy compared with that in  $\text{Pd}_{1.0}/\text{graphene}$  and  $\text{Fe}_{1.0}/\text{graphene}$  catalysts. It suggested that a bimetallic Pd–Fe miscible phase was partially formed that caused the unique surface electronic structure in the  $\text{Pd}_{0.5}\text{Fe}_{0.5}/\text{graphene}$  catalyst [38,39]. Combined with the analysis of XRD spectra (Fig. 1a), HR-TEM images (Fig. 2d–f) and XPS spectra (Fig. 3), Fe homogeneously entered into the lattice of Pd and Pd–Fe alloy has been formed in  $\text{Pd}_{0.5}\text{Fe}_{0.5}/\text{graphene}$  catalyst, which could be hardly obtained by chemical reduction process due to the fast reduction rate [10,33].

Fig. 4 summarizes the complete synthetic process. Under continuous UV sensitization, a charge transfer transition occurs in the W–O–W bonds of HPW, resulting in the excited-state ( $\text{HPW}^*$ ),  $\text{HPW}^*$  is reduced to  $\text{HPW}^-$  with the participation of  $\text{Me}_2\text{CHOH}$  as an electron donor under UV irradiation.  $\text{HPW}^-$  has powerful reduc-

tion abilities and is able to reduce GO to graphene. Simultaneously, bimetallic Pd–Fe NPs are formed and loaded onto the surface of the graphene sheets. The reaction may be represented by the following equations [34,40]:



Fig. 3c shows the XPS spectra of the Fe 2p signals presented by the  $\text{Fe}_{1.0}/\text{graphene}$  and  $\text{Pd}_{0.5}\text{Fe}_{0.5}/\text{graphene}$  catalysts. The peaks at 706.6 eV ( $\text{Fe}^0 2p_{3/2}$ ), 712.5 eV ( $\text{Fe}^{3+} 2p_{3/2}$ ), 717.9 eV ( $\text{Fe}^0 2p_{1/2}$ ), and 723.25 eV ( $\text{Fe}^{3+} 2p_{1/2}$ ) indicate that  $\text{Fe}^0$  and  $\text{Fe}^{3+}$  species are present in the  $\text{Fe}_{1.0}/\text{graphene}$  catalyst. The  $\text{Pd}_{0.5}\text{Fe}_{0.5}/\text{graphene}$  catalyst also presents peaks for  $\text{Fe}^0$  and  $\text{Fe}^{3+}$  species with binding energies of 706 eV ( $\text{Fe}^0 2p_{3/2}$ ), 712.4 eV ( $\text{Fe}^{3+} 2p_{3/2}$ ), 717.4 eV ( $\text{Fe}^0 2p_{1/2}$ ), and 722.8 eV ( $\text{Fe}^{3+} 2p_{1/2}$ ). It is noteworthy that all the samples contain significant amounts of cationic metallic species ( $\text{Pd}^{2+}$  and/or  $\text{Fe}^{3+}$ ), except the metallic Pd ( $\text{Pd}^0$ ) and/or metallic Fe ( $\text{Fe}^0$ ). It has been reported that UV-assisted reduction of GO to graphene sheets with HPW produces a significant number of carbon vacancies and surface defects, which further provides blinding sites for NP loading [33,34]. Therefore, such a high  $\text{Pd}^{2+}$  content might result from the electron transfer from the Pd NPs to the graphene owing to the strong metal–support interaction in the catalysts [1,13].

The  $\text{Pd}^{2+}/\text{Pd}^0$  and  $\text{Fe}^{3+}/\text{Fe}^0$  ratios for different catalysts were calculated. The values of the  $\text{Pd}^{2+}/\text{Pd}^0$  and  $\text{Fe}^{3+}/\text{Fe}^0$  ratios are 0.53 and 1.45, respectively, for  $\text{Pd}_{0.5}\text{Fe}_{0.5}/\text{graphene}$ , which are smaller than those for  $\text{Pd}_{1.0}/\text{graphene}$  (0.64) and  $\text{Fe}_{1.0}/\text{graphene}$  (3.25). Thus,  $\text{Pd}^0$  and  $\text{Fe}^{3+}$  species are the main components of the corresponding catalysts. The decreasing  $\text{Pd}^{2+}/\text{Pd}^0$  and  $\text{Fe}^{3+}/\text{Fe}^0$  ratios imply that the addition of Fe improves the percentages of  $\text{Pd}^0$  and  $\text{Fe}^0$ , which could benefit the catalytic process [10,22]. This may be attributed

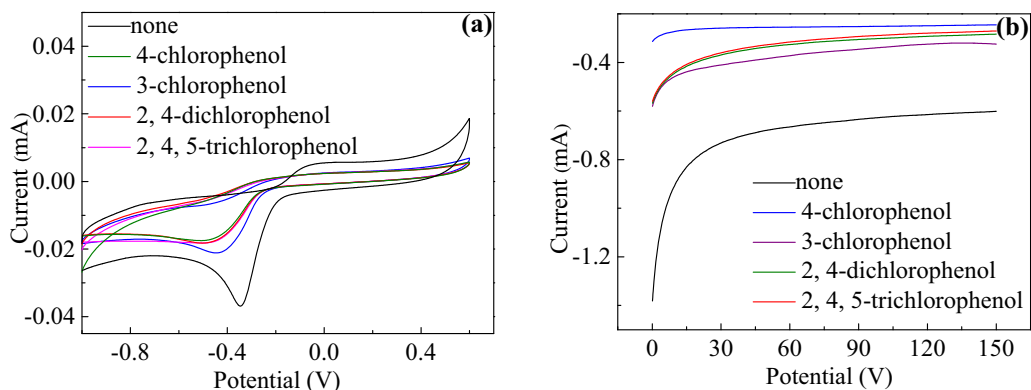


Fig. 9. CV curves (a) and i-t curves (b) of  $\text{Pd}_{0.5}\text{Fe}_{0.5}/\text{graphene}$  catalyst for the oxidation of different CPs ( $100 \text{ mg L}^{-1}$ );  $v = 100 \text{ mV s}^{-1}$ .

to partial  $\text{Pd}^{2+}$  loading at the carbon vacancies and surface defects being substituted by Fe to form  $\text{Fe}^{3+}$ .

### 3.2. Electrocatalytic properties of different catalysts

Cyclic voltammetry was employed to characterize the electrochemical properties of the  $\text{Pd}_{1.0}/\text{graphene}$ ,  $\text{Fe}_{1.0}/\text{graphene}$ , and  $\text{Pd}_{0.5}\text{Fe}_{0.5}/\text{graphene}$  catalysts. The resulting voltammetric responses of the catalysts upon hydrogen adsorption (pH 12.8,  $0.5 \text{ mol L}^{-1}$   $\text{Na}_2\text{SO}_4$ , scan rate  $50 \text{ mV s}^{-1}$ , feeding with  $\text{H}_2$ ) are illustrated in Fig. 5a. The  $\text{Pd}_{0.5}\text{Fe}_{0.5}/\text{graphene}$  catalyst shows a high reduction peak attributed to the formation of adsorbed hydrogen ( $\text{H}_{\text{ads}}$ ) with a peak current of  $0.117 \text{ mA}$  at  $\sim -0.345 \text{ V}$ , which is different to the  $\text{Pd}_{1.0}/\text{graphene}$  and  $\text{Fe}_{1.0}/\text{graphene}$  catalysts. No obvious current response is observed in the CV curves of  $\text{Pd}_{1.0}/\text{graphene}$  and  $\text{Fe}_{1.0}/\text{graphene}$ . However, the current for  $\text{Pd}_{1.0}/\text{graphene}$  increases rapidly from  $0 \text{ V}$  to  $-0.8 \text{ V}$ , which may also be due to hydrogen adsorption, while  $\text{Fe}_{1.0}/\text{graphene}$  shows no significant change in current. It was noteworthy that the peak current of  $\text{Pd}_{0.5}\text{Fe}_{0.5}/\text{graphene}$  catalyst ( $0.117 \text{ mA}$ ) obtained in hydrogen adsorption was significantly higher than the previous catalyst ( $0.073 \text{ mA}$ ) prepared by traditional chemical method [10].

The process of  $\text{H}_{\text{ads}}$  formation upon  $\text{H}_2$  feeding has been rationalized in two ways in the previous literature [41]: (1) hydrogen atoms from the electrolysis of water are adsorbed onto the Pd surface; and (2) the hydrogen atoms from the  $\text{H}_2$  gas feed are adsorbed on the Pd surface immediately. The  $\text{H}_{\text{ads}}$  replaces the chlorine atom in the adsorbed chlorinated organic substrates during the ECH process. Based on this,  $\text{Pd}_{0.5}\text{Fe}_{0.5}/\text{graphene}$  shows the potential for higher electrocatalytic activity in dechlorination owing to its higher hydrogen adsorption current, which is directly related to the electrocatalytic activity [16].

In fact, organic pollutants are mainly degraded by the indirect electro-oxidation process during the combined electrochemical reduction and oxidation, which involves  $\text{H}_2\text{O}_2$  electro-generation by the electrochemical reduction of  $\text{O}_2$  at the cathode [2]. Generally, the electro-generation of  $\text{H}_2\text{O}_2$  is positively correlated to the performance of the catalyst [9,42]. Therefore, the electrocatalytic activity of the prepared catalysts for electrochemical reduction of  $\text{O}_2$  to  $\text{H}_2\text{O}_2$  was investigated to evaluate their potential application in the indirect electro-oxidation of CPs. Fig. 5b shows the CV curves of the  $\text{Pd}_{1.0}/\text{graphene}$ ,  $\text{Fe}_{1.0}/\text{graphene}$ , and  $\text{Pd}_{0.5}\text{Fe}_{0.5}/\text{graphene}$  catalysts under  $\text{O}_2$  in a  $\text{Na}_2\text{SO}_4$  electrolyte ( $0.05 \text{ mol L}^{-1}$ ) at pH 12.8. High reduction peaks at about  $-0.300\text{--}0.400 \text{ V}$  are observed for the oxygen-saturated alkaline solution. According to the redox potential, these peaks indicate the electrochemical reaction of the two-electron reduction of  $\text{O}_2$  to  $\text{H}_2\text{O}_2$  [42]. The reduction peak current of the  $\text{Pd}_{0.5}\text{Fe}_{0.5}/\text{graphene}$  catalyst is  $0.038 \text{ mA}$  at

$-0.347 \text{ V}$ , much higher than that of  $\text{Pd}_{1.0}/\text{graphene}$  ( $0.027 \text{ mA}$ ) and  $\text{Fe}_{1.0}/\text{graphene}$  ( $0.024 \text{ mA}$ ) at  $-0.385 \text{ V}$ . The higher peak current and less negative potential for the  $\text{Pd}_{0.5}\text{Fe}_{0.5}/\text{graphene}$  catalyst suggest that  $\text{Pd}_{0.5}\text{Fe}_{0.5}/\text{graphene}$  has a higher electrocatalytic activity than  $\text{Pd}_{1.0}/\text{graphene}$  and  $\text{Fe}_{1.0}/\text{graphene}$  in the two-electron reduction of  $\text{O}_2$  to  $\text{H}_2\text{O}_2$ , and that electron transfer for the reduction of  $\text{O}_2$  is easier when using the  $\text{Pd}_{0.5}\text{Fe}_{0.5}/\text{graphene}$  catalyst. In addition, the peak current of  $\text{Pd}_{0.5}\text{Fe}_{0.5}/\text{graphene}$  catalyst ( $0.038 \text{ mA}$ ) was higher than that of the same catalyst ( $0.031 \text{ mA}$ ) synthesized by chemical reduction reported in our previous work [10]. The comparative results confirm the feasibility and validity of UV-irradiation with HPW to prepare graphene-supported catalysts.

In comparison with the reduction peak currents and potentials of the other catalysts (shown in Fig. 5 and Fig. S6), the  $\text{Pd}_{0.5}\text{Fe}_{0.5}/\text{graphene}$  catalyst shows the highest peak current and lowest peak potential. This indicates that the  $\text{Pd}_{0.5}\text{Fe}_{0.5}/\text{graphene}$  catalyst exhibits the best potential for catalytic activity in the indirect electro-oxidation of CPs. As the analysis of XPS spectra proposed above, the addition of Fe in Pd-Fe alloy NPs could improve the percentages of  $\text{Pd}^0$  and  $\text{Fe}^0$ , which could benefit for hydrogen adsorption and the  $\text{O}_2$  reduction process. In addition, the synergistic effect in bimetallic Pd-Fe could play a critical role in electrocatalysis process [22].

Furthermore, as shown in Fig. 6, the reductive peak current with the  $\text{Pd}_{0.5}\text{Fe}_{0.5}/\text{graphene}$  catalyst is  $0.038 \text{ mA}$  upon feeding with  $\text{O}_2$ , higher than that upon feeding with air ( $0.013 \text{ mA}$ ), and there is no reduction peak upon feeding with  $\text{N}_2$ . This is attributed to the enhancement of the reduction of  $\text{O}_2$  when dissolved oxygen easily diffuses to the electrode surface, which is promoted by feeding with  $\text{O}_2$  [43]. The onset of reduction shifts to positive potentials at high pH (in Fig. 7), which indicates that the  $\text{O}_2$  is reduced more easily in the alkaline solution [44].

Cyclic voltammetry of the three catalysts at different scan rates ( $50\text{--}800 \text{ mV s}^{-1}$ ) was carried out to provide more insight into the role of the  $\text{Pd}_{0.5}\text{Fe}_{0.5}/\text{graphene}$  catalyst. The resulting voltammetric responses of the  $\text{Pd}_{0.5}\text{Fe}_{0.5}/\text{graphene}$ ,  $\text{Pd}_{1.0}/\text{graphene}$ , and  $\text{Fe}_{1.0}/\text{graphene}$  catalysts in alkaline solution ( $0.5 \text{ mol L}^{-1}$   $\text{Na}_2\text{SO}_4$ , pH 12.8) are shown in Fig. 8. When the sweep rate is increased from  $50 \text{ mV s}^{-1}$  to  $800 \text{ mV s}^{-1}$ , the potentials shift negatively, and the reductive peak intensity increases. This means that the electrochemical reduction of  $\text{O}_2$  is an irreversible process [45]. The peak current presents a linear relationship with the log of the scan rate (insets of Fig. 8). Thus, the electrochemical reductive reaction of  $\text{O}_2$  in this work is a typical diffusion-controlled electrochemical process [46,47], which indicates that the reaction rate is controlled by the diffusion of  $\text{O}_2$  in the electrolyte rather than the number of active sites on the Pd-Fe nanoparticle surfaces. The peak current can be calculated as:  $I_p = 2.99 \times 10^5 n(\alpha n)^{1/2} A c D^{1/2} v^{1/2}$  [48].

The equation can be simplified to:  $I_p = kv^{1/2}$  [47]. Since A and C are the invariants in this study,  $k$  (the fitting line slopes of  $I_p$  vs.  $v^{1/2}$ ), which expresses the mass transfer rate of the samples, is a coefficient related only to D. Based on this, the mass transfer is faster if the value of  $k$  is higher. The calculated values of  $k$  follow the sequence  $\text{Pd}_{0.5}\text{Fe}_{0.5}/\text{graphene}$  (0.379) >  $\text{Pd}_{1.0}/\text{graphene}$  (0.178) >  $\text{Fe}_{1.0}/\text{graphene}$  (0.175). The highest  $k$  for  $\text{Pd}_{0.5}\text{Fe}_{0.5}/\text{graphene}$  further demonstrates that the co-modified Pd and Fe enhance the mass transfer rate. The surfaces of these catalysts provide the reaction site and the location for the supply and reception of electrons. The  $\text{Pd}_{0.5}\text{Fe}_{0.5}/\text{graphene}$  catalyst, which features highly abundant, small, and well-dispersed Pd-Fe NPs, may have a significant activation effect on the molecules or ions participating in the electrochemical reaction [10].

### 3.3. Electrochemical activity of $\text{Pd}_{0.5}\text{Fe}_{0.5}/\text{graphene}$ catalyst for CPs

Based on the above results, the  $\text{Pd}_{0.5}\text{Fe}_{0.5}/\text{graphene}$  catalyst should exhibit a higher catalytic activity than the other catalysts. Therefore, this catalyst was selected for the indirect electrochemical oxidation of CPs. The electrochemical properties of the prepared  $\text{Pd}_{0.5}\text{Fe}_{0.5}/\text{graphene}$  catalyst for the indirect electrochemical oxidation of CPs were characterized using CV in basic solutions containing different CPs. As shown in Fig. 9a, the reduction peak currents for four CPs decreased in the order 3-CP (0.0214 mA) > 2,4,5-TCP (0.0190 mA) > 2,4-DCP (0.0188 mA) > 4-CP (0.0178 mA). Due to the electron transfer from the electrode surface to the CPs in the ECH process, it was harder for the reduction of  $\text{O}_2$  to  $\text{H}_2\text{O}_2$  [49]. Since different values of peak current represent the resistant extent for the CPs degradation, the  $\text{Pd}_{0.5}\text{Fe}_{0.5}/\text{graphene}$  electrode exhibited superior electro-oxidation for 3-CP degradation than that of the other CPs. In addition, the peak potentials are  $-0.36$ ,  $-0.37$ ,  $-0.38$ , and  $-0.39$  V in basic solutions containing 3-CP, 2,4,5-TCP, 2,4-DCP, and 4-CP, respectively. It indicated that the  $\text{O}_2$  reduction to  $\text{H}_2\text{O}_2$  took place easier with 3-CP than the other CPs. The energy of highest occupied molecular orbital ( $E_{\text{HOMO}}$ ) of CPs has been calculated and shown as follows: 2,4,5-TCP (0.555) > 2,4-CP (0.245) > 4-DCP (0.052) > 3-CP (0.0041) [50]. With the smaller  $E_{\text{HOMO}}$  value, CPs showed stronger ability for accepting electrons. It also indicated that 3-CP was easy to be degraded compared with the other CPs.

The chronoamperometry curves are shown in Fig. 9b. The current values display a decreasing trend in all the curves. The stabilized current values appearing after  $\sim 120$  s are 0.41, 0.40, 0.39, and 0.34 mA in the basic solutions containing 3-CP, 2,4,5-TCP, 2,4-DCP, and 4-CP, respectively. Attention should be given to the relationship between the diffusion rates of the electroactive substance and the chronoamperometry plots according to the Cottrell equation. Under the same initial concentration and reaction time, the diffusion rate is proportional to the contact current [51].

## 4. Conclusions

A simple and green method for the syntheses of graphene-supported Pd, Fe, and bimetallic Pd-Fe NP catalysts based on UV-assisted photocatalytic reduction was presented, and the resultant catalysts were characterized by XRD, SEM, TEM, AFM, and XPS. These analyses showed that the bimetallic Pd-Fe NPs in the  $\text{Pd}_{0.5}\text{Fe}_{0.5}/\text{graphene}$  catalyst have appropriate sizes of  $6.75 \pm 0.25$  nm and superior dispersion on the graphene sheets, providing more active sites, which could be beneficial to electrochemical reactions. The introduction of Fe to the NPs improved their dispersion, but did not significantly affect their sizes. Through comparing the CV results for catalysts with different metal loading

ratios, the  $\text{Pd}_{0.5}\text{Fe}_{0.5}/\text{graphene}$  catalyst was found to exhibit higher potential electrocatalytic activity for dechlorination owing to its higher hydrogen adsorption current and efficiency for indirect-oxidation, as indicated by its higher reduction capacity for  $\text{O}_2$  to  $\text{H}_2\text{O}_2$ . CV at different scan rates (50–800 mV s $^{-1}$ ) performed in alkaline solution (0.5 mol L $^{-1}$   $\text{Na}_2\text{SO}_4$ , pH 12.8) revealed that the reaction rate with the  $\text{Pd}_{0.5}\text{Fe}_{0.5}/\text{graphene}$  catalyst was controlled by the diffusion of  $\text{O}_2$  in the electrolyte rather than the number of active sites on the Pd-Fe nanoparticle surface. The calculated value of  $k$  for the samples followed the sequence  $\text{Pd}_{0.5}\text{Fe}_{0.5}/\text{graphene}$  (0.379) >  $\text{Pd}_{1.0}/\text{graphene}$  (0.178) >  $\text{Fe}_{1.0}/\text{graphene}$  (0.175), indicating that the co-modified Pd-Fe exhibits an enhanced mass transfer rate. The peak currents for  $\text{Pd}_{0.5}\text{Fe}_{0.5}/\text{graphene}$  with CPs decreased in the order 3-CP (0.0214 mA) > 2,4,5-TCP (0.0190 mA) > 2,4-DCP (0.0188 mA) > 4-CP (0.0178 mA), indicating that the amount of  $\text{H}_2\text{O}_2$  produced decreases in that order.

## Acknowledgments

This work was supported by the Fundamental Research Funds for the Central Universities (No. 2016ZCQ03), the National Natural Science Foundation of China (No. 51278053 and 21373032).

## Appendix A. Supplementary data

Supplementary data associated with this article can be found, in the online version, at <http://dx.doi.org/10.1016/j.apcatb.2016.10.036>.

## References

- [1] J. Zhou, K. Wu, W.J. Wang, Z.Y. Xu, H.Q. Wan, S.R. Zheng, Pd supported on boron-doped mesoporous carbon as highly active catalyst for liquid phase catalytic hydrodechlorination of 2, 4-dichlorophenol, *Appl. Catal. A: Gen.* 470 (2014) 336as–343.
- [2] H. Wang, J.L. Wang, Electrochemical degradation of 4-chlorophenol using a novel Pd/C gas-diffusion electrode, *Appl. Catal. B: Environ.* 77 (2007) 58–65.
- [3] Z.R. Sun, X.F. Wei, H.T. Shen, X. Hu, Preparation of palladium–nickel loaded titanium electrode with surfactant assistance and its application in pentachlorophenol reductive dechlorination, *Sep. Purif. Technol.* 124 (2014) 224–230.
- [4] Y.Y. Liang, Y.G. Li, H.L. Wang, H.J. Dai, Strongly coupled inorganic/nanocarbon hybrid materials for advanced electrocatalysis, *J. Am. Chem. Soc.* 135 (2013) 2013–2036.
- [5] Z.Y. Bian, Y. Bian, H. Wang, A.Z. Ding, Synthesis of Pd nanoparticles decorated with graphene and their application in electrocatalytic degradation of 4-chlorophenol, *J. Nanosci. Nanotechnol.* 14 (2014) 7279–7285.
- [6] A.A. Peverly, T.L. Dresbach, K.N. Knust, T.F. Koss, M.K. Longmire, D.G. Peters, Electrochemical reduction of 2,4-dichloro-1-(4-chloro-2-methoxyphenoxy) benzene (methyl triclosan) at glassy carbon cathodes in dimethylformamide, *J. Electroanal. Chem.* 731 (2014) 1–5.
- [7] A.A. Isse, B.B. Huang, C. Durante, A. Gennaro, Electrocatalytic dechlorination of volatile organic compounds at a copper cathode. Part I: polychloromethanes, *Appl. Catal. B: Environ.* 126 (2012) 347–354.
- [8] Z.R. Sun, H.T. Shen, X.F. Wei, X. Hu, Electrocatalytic hydrogenolysis of chlorophenols in aqueous solution on  $\text{Pd}_{58}\text{Ni}_{42}$  cathode modified with PPy and SDBS, *Chem. Eng. J.* 241 (2014) 433–442.
- [9] H. Wang, X.J. Wei, Z.Y. Bian, Degradation of 4-chlorophenol by the anodic–cathodic cooperative effect with a Pd/MWNT gas-diffusion electrode, *Water Sci. Technol.* 65 (2012) 2010–2015.
- [10] Q. Shi, H. Wang, S.L. Liu, L. Pang, Z.Y. Bian, Electrocatalytic reduction-oxidation of chlorinated phenols using a nanostructured Pd-Fe modified graphene catalyst, *Electrochim. Acta* 178 (2015) 92–100.
- [11] D.M. Gattia, M.V. Antisari, R. Marazzi, AC arc discharge synthesis of single-walled nanohorns and highly convoluted graphene sheets, *Nanotechnology* 18 (2007) 255604.
- [12] H.Y. Deng, G.Y. Fan, C.Y. Wang, L. Zhang, Aqueous phase catalytic hydrodechlorination of 4-chlorophenol over palladium deposited on reduced graphene oxide, *Catal. Commun.* 46 (2014) 219–223.
- [13] P. Wang, Z.G. Liu, X. Chen, F.L. Meng, J.H. Liu, X.J. Huang, UV irradiation synthesis of an Au–graphene nanocomposite with enhanced electrochemical sensing properties, *J. Mater. Chem. A* (2013) 9189–9195.
- [14] A. Dutta, J. Ouyang, Enhanced electrocatalytic performance on polymer-stabilized graphene decorated with alloy nanoparticles for ethanol oxidation reaction in alkaline media, *Appl. Catal. B: Environ.* 158 (2014) 119–128.

[15] S.Z. Butler, S.M. Hollen, L.Y. Cao, Y. Cui, J.A. Gupta, H.R. Gutierrez, T.F. Heinz, S.S. Hong, J.X. Huang, A.F. Ismach, E. Johnston-Halperin, M. Kuno, V.V. Plashnitsa, R.D. Robinson, R.S. Ruoff, S. Salahuddin, J. Shan, L. Shi, M.G. Spencer, M. Terrones, W. Windl, J.E. Goldberger, Progress, challenges, and opportunities in two-dimensional materials beyond graphene, *ACS Nano* 7 (2013) 2898–2926.

[16] C. Luo, Z. Chen, D.L. Wu, L.M. Ma, Electrochemical reductive degradation of chlorobenzene using galvanically replaced Pd/Fe nanoscale particles, *Chem. Eng. J.* 241 (2014) 376–383.

[17] Y. Kim, Y. Noh, E.J. Lim, S. Lee, S.M. Choi, W.B. Kim, Star-shaped Pd@Pt core-shell catalysts supported on reduced graphene oxide with superior electrocatalytic performance, *J. Mater. Chem. A* 2 (2014) 6976–6986.

[18] Y.B. Huang, S.J. Liu, Z.J. Lin, W.J. Li, X.F. Li, R. Cao, Facile synthesis of palladium NPs encapsulated in amine-functionalized mesoporous metal–organic frameworks and catalytic for dehalogenation of aryl chlorides, *J. Catal.* 293 (2012) 111–117.

[19] M.O. Nutt, K.N. Heck, P. Alvarez, M.S. Wong, Improved Pd-on-Au bimetallic nanoparticle catalysts for aqueous-phase trichloroethene hydrodechlorination, *Appl. Catal. B: Environ.* 69 (2006) 115–125.

[20] V. Simagina, V. Likhobolov, G. Bergeret, M.T. Gimenez, A. Renouprez, Catalytic hydrodechlorination of hexachlorobenzene on carbon supported Pd–Ni bimetallic catalysts, *Appl. Catal. B: Environ.* 40 (2003) 293–304.

[21] J.K. Kim, J.K. Lee, K.H. Kang, J.C. Song, I.K. Song, Selective cleavage of C–O bond in benzyl phenyl ether to aromatics over Pd–Fe bimetallic catalyst supported on ordered mesoporous carbon, *Appl. Catal. A: Gen.* 498 (2015) 142–149.

[22] J.M. Sun, A.M. Karim, H. Zhang, L. Kovarik, X.H.S. Li, A.J. Hensley, J.S. McEwen, Y. Wang, Carbon-supported bimetallic Pd–Fe catalysts for vapor-phase hydrodeoxygenation of guaiacol, *J. Catal.* 306 (2013) 47–57.

[23] W.Q. Feng, L. Yang, N. Cao, C. Du, H.M. Dai, W. Luo, G.Z. Cheng, In situ facile synthesis of bimetallic CoNi catalyst supported on graphene for hydrolytic dehydrogenation of amine borane, *Int. J. Hydrogen Energy* 39 (2014) 3371–3380.

[24] A.Z. Li, X. Zhao, Y.N. Hou, H.J. Liu, L.Y. Wu, J.H. Qu, The electrocatalytic dechlorination of chloroacetic acids at electrodeposited Pd/Fe-modified carbon paper electrode, *Appl. Catal. B: Environ.* 111 (2012) 628–635.

[25] Z.B. Peng, Z.B. Yu, L. Wang, Y.P. Hou, Y.F. Shi, L.D. Wu, Z.C. Li, Facile synthesis of Pd–Fe nanoparticles modified Ni foam electrode and its behaviors in electrochemical reduction of tetrabromobisphenol A, *Mater. Lett.* 166 (2016) 300–303.

[26] X.Y. Wang, L. Le, P.J.J. Alvarez, F. Li, K.Q. Liu, Synthesis and characterization of green agents coated Pd/Fe bimetallic nanoparticles, *J. Taiwan Inst. Chem. E* 50 (2015) 297–305.

[27] Y.H. Shih, M.Y. Chen, Y.F. Su, C.P. Tso, Concurrent oxidation and reduction of pentachlorophenol by bimetallic zerovalent Pd/Fe nanoparticles in an oxic water, *J. Hazard. Mater.* 301 (2016) 416–423.

[28] F. Zhang, F.M. Yasin, X.J. Chen, J.X. Mo, C.L. Raston, H.B. Zhang, Functional noble metal nanostructures involving pyrene-conjugated-hyaluronan stabilised reduced graphene oxide, *RSC Adv.* 3 (2013) 25166–25174.

[29] H.L. Li, S.P. Pang, S. Wu, X.L. Feng, K. Muellen, C. Bubeck, Layer-by-layer assembly and UV photoreduction of graphene–polyoxometalate composite films for electronics, *J. Am. Chem. Soc.* 133 (2011) 9423–9429.

[30] Y. Matsuo, K. Iwasa, T. Mimura, Y. Tachibana, Preparation of pillared carbon thin films from the reduction of silylated graphite oxide by UV light irradiation and their size selective electrical response to various molecules, *Carbon* 75 (2014) 271–276.

[31] G. Williams, B. Seger, P.V. Kamat, TiO<sub>2</sub>–graphene nanocomposites. UV-assisted photocatalytic reduction of graphene oxide, *ACS Nano* 2 (2008) 1487–1491.

[32] H. Gu, Y. Yang, J.X. Tian, G.Y. Shi, Photochemical synthesis of noble metal (Ag, Pd Au, Pt) on graphene/ZnO multihybrid nanoarchitectures as electrocatalysis for H<sub>2</sub>O<sub>2</sub> reduction, *ACS Appl. Mater. Interfaces* 5 (2013) 6762–6768.

[33] G.H. Moon, Y. Park, W. Kim, W. Choi, Photochemical loading of metal nanoparticles on reduced graphene oxide sheets using phosphotungstate, *Carbon* 49 (2011) 3454–3462.

[34] R. Pasricha, S. Gupta, A.G. Joshi, N. Bahadur, D. Haranath, K.N. Sood, S. Singh, S. Singh, Directed nanoparticle reduction on graphene, *Mater. Today* 15 (2012) 118–125.

[35] W.S. Hummers, R.E. Offeman, Preparation of graphitic oxide, *J. Am. Chem. Soc.* 80 (1958) (1339–1339).

[36] D.C. Marcano, D.V. Kosynkin, J.M. Berlin, A. Sinitskii, Z.Z. Sun, A. Slesarev, L.B. Alemany, W. Lu, J.M. Tour, Improved synthesis of graphene oxide, *ACS Nano* 4 (2010) 4806–4814.

[37] R.F. Nie, D. Liang, L. Shen, J. Gao, P. Chen, Z.Y. Hou, Selective oxidation of glycerol with oxygen in base-free solution over MWCNTs supported PtSb alloy nanoparticles, *Appl. Catal. B: Environ.* 127 (2012) 212–220.

[38] J.W. Hong, Y. Kim, D.H. Wi, S. Lee, S.U. Lee, Y.W. Lee, S.I. Choi, S.W. Han, Ultrathin free-standing trnary-alloy nanosheets, *Angew. Chem. Int. Ed.* 55 (2016) 2753–2758.

[39] Y.L. Zheng, S.L. Zhao, S.L. Liu, H.H. Yin, Y.Y. Chen, J.C. Bao, M. Han, Z.H. Dai, Component-controlled synthesis and assembly of Cu–Pd nanocrystals on graphene for oxygen reduction reaction, *ACS Appl. Mater. Interfaces* 7 (2015) 5347–5357.

[40] R.F. Renneke, C.L. Hill, Homogeneous catalytic photochemical functionalization of alkanes by polyoxometalates, *J. Am. Chem. Soc.* 108 (1986) 3528–3529.

[41] L. Chan, S. Pyun, Impedance analysis of hydrogen absorption reaction on Pd membrane electrode in 0.1 M LiOH solution under permeable boundary conditions Pergamon, *Electrochim. Acta* 39 (1994) 363–373.

[42] H. Wang, J.L. Wang, Electrochemical degradation of 2,4-dichlorophenol on a palladium modified gas-diffusion electrode, *Electrochim. Acta* 53 (2008) 6402–6409.

[43] S. Marini, P. Salvini, P. Nelli, R. Pesenti, M. Villa, Y. Kirov, Oxygen evolution in alkali with gas diffusion electrodes, *Int. J. Hydrogen Energy* 38 (2013) 11496–11506.

[44] S. Salome, R. Rego, M.C. Oliveira, Development of silver-gas diffusion electrodes for the oxygen reduction reaction by electrodeposition, *Mater. Chem. Phys.* 143 (2013) 109–115.

[45] N. Maleki, A. Safavi, E. Farjam, F. Tajabadi, Palladium, nanoparticle decorated carbon ionic liquid electrode for highly efficient electrocatalytic oxidation and determination of hydrazine, *Anal. Chim. Acta* 611 (2008) 151–155.

[46] L. La-Torre-Riveros, K. Soto, M.A. Scibioh, C.R. Cabrera, Electrophoretically fabricated diamond nanoparticle-based electrodes, *J. Electrochem. Soc.* 157 (2010) B831–B836.

[47] L.M. Chang, Y. Zhou, X.Y. Duan, W. Liu, D.D. Xu, Preparation and characterization of carbon nanotube and Bi co-doped PbO<sub>2</sub> electrode, *J. Taiwan Inst. Chem. E* 45 (2014) 1338–1346.

[48] H.J. Zhang, J.S. Huang, H.Q. Hou, T.Y. You, Electrochemical detection of hydrazine based on electrospun palladium nanoparticle/carbon nanofibers, *Electroanal.* 21 (2009) 1869–1874.

[49] K. Mackenzie, H. Frenzel, F.D. Kopinke, Hydrodehalogenation of halogenated hydrocarbons in water with Pd catalysts: reaction rates and surface competition, *Appl. Catal. B: Environ.* 63 (2006) 161–167.

[50] G.S. Liu, J.G. Yu, QSAR analysis of soil sorption coefficients for polar organic chemicals: substituted anilines and phenols, *Water Res.* 39 (2005) 2048–2055.

[51] E. Wierzbicka, G.D. Sulka, Nanoporous spongelike Au–Ag films for electrochemical epinephrine sensing, *J. Electroanal. Chem.* 762 (2016) 43–50.